Supplementary Information

Smartphone-Assisted Natural Rubber Cryogel Electrodes with Copper Oxide–Densely Decorated Multi-Walled Carbon Nanotubes for On-Site Glucose Sensing

Panita Kongsune [ab], Natsinath Kaewprachum [a], Wanrudee Hiranrat [ab], Warakorn Witsapan [ab], Panita Sumanatrakul [c], Apon Numnuam [d], Titilope John Jayeoye [e] and Tawatchai Kangkamano [ab]*

[a] *Department of Chemistry, Faculty of Science and Digital Innovation, Thaksin University, Phatthalung Campus, Papayom, Phatthalung 93210, Thailand*

[b] *Innovative Material Chemistry for Environment Center, Thaksin University, Phattalung, 93210, Thailand*

[c] *Rubber and Polymer Engineering Program, Faculty of Engineering, Thaksin University, Phatthalung Campus, Papayom, Phatthalung 93210, Thailand*

[d] *Department of Chemistry, Faculty of Science, Prince of Songkla University 90110, Hat Yai, Songkhla, Thailand*

[e] *Department of Chemistry, Biochemistry and Molecular Biology, Federal University Ndufu Alike Ikwo, Abakaliki, Ebonyi State, Nigeria*

* *Corresponding author at: Department of Chemistry, Faculty of Science and Digital Innovation, Thaksin University, Phatthalung Campus, Papayom, Phatthalung, 93210, Thailand*

Tel.: +66 74 609607; fax: +66 74 609607

E-mail address: ktawatchai@tsu.ac.th; tkangkamano@yahoo.com

Fig. S1 Dynamic light scattering (DLS) size distribution profiles (Size distribution by intensity) of (A) Triton X-114 micelles and (B) Cu^{2+}-loaded Triton X-114 micelles. Upon incorporation of Cu^{2+} ions, the hydrodynamic diameter decreased from approximately 50.47 nm to 40.80 nm, indicating coordination interaction between Cu^{2+} ions and the polyethylene oxide (PEO) chains of Triton X-114. The reduction in micellar size suggests an altered core microenvironment and decreased aggregation number after Cu^{2+} incorporation, supporting the formation of Cu^{2+}-loaded micelles that function as soft nanoreactors during CuO nanoparticle synthesis.

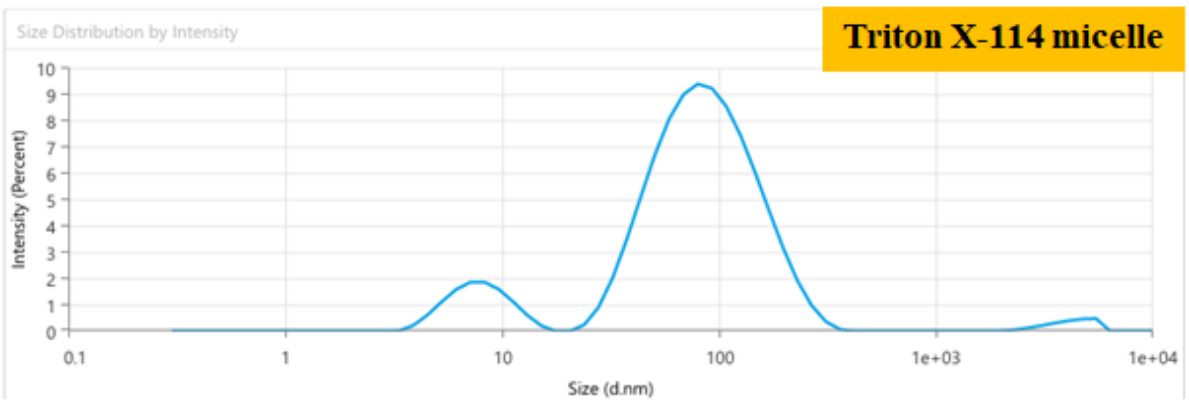

Z-Average (nm) ≈ 50.47 nm
Polydispersity Index (PI) ≈ 0.5999

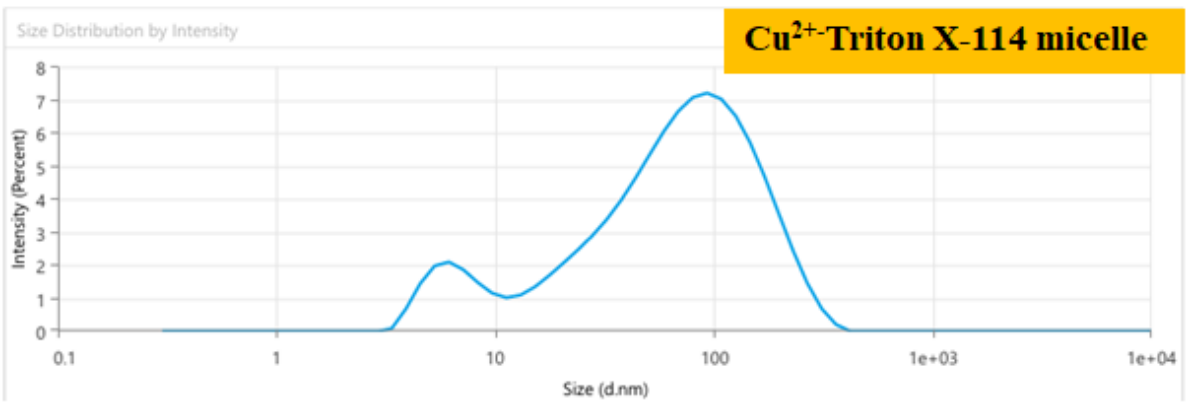

Z-Average (nm) ≈ 40.80 nm
Polydispersity Index (PI) ≈ 0.5977

Fig. S2 Representative surface morphology of the CuO@f-MWCNTs–RB cryogel (top) used for pore size measurement and the corresponding pore size distribution histogram (bottom). The pore diameters reveal a broad size distribution of approximately 4–53 µm, with an average pore diameter of ~18±11 µm (N = 80).

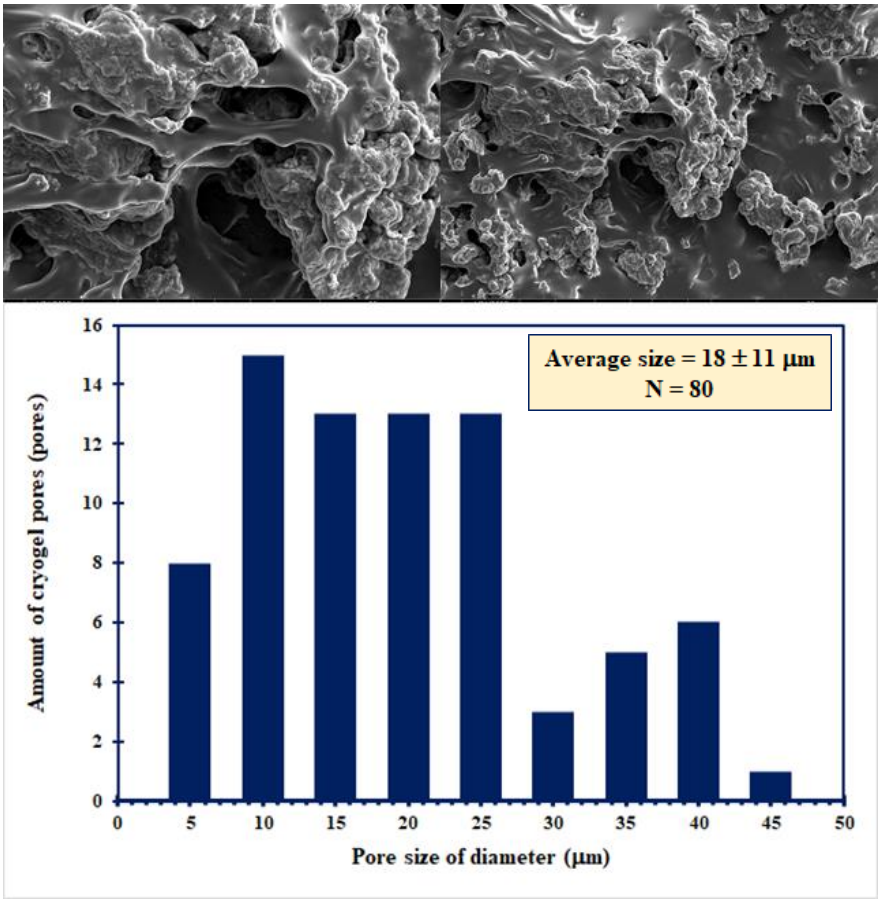

Fig. S3 Cyclic voltammograms recorded for (A) CuO@f-MWCNTs–RB non-cryogel/SPE and (B) CuO@f-MWCNTs–RB cryogel/SPE in the presence of glucose at concentrations ranging from 0.0 to 6.0 mM in 0.10 M NaOH at a scan rate of 100 mV s^{-1}.

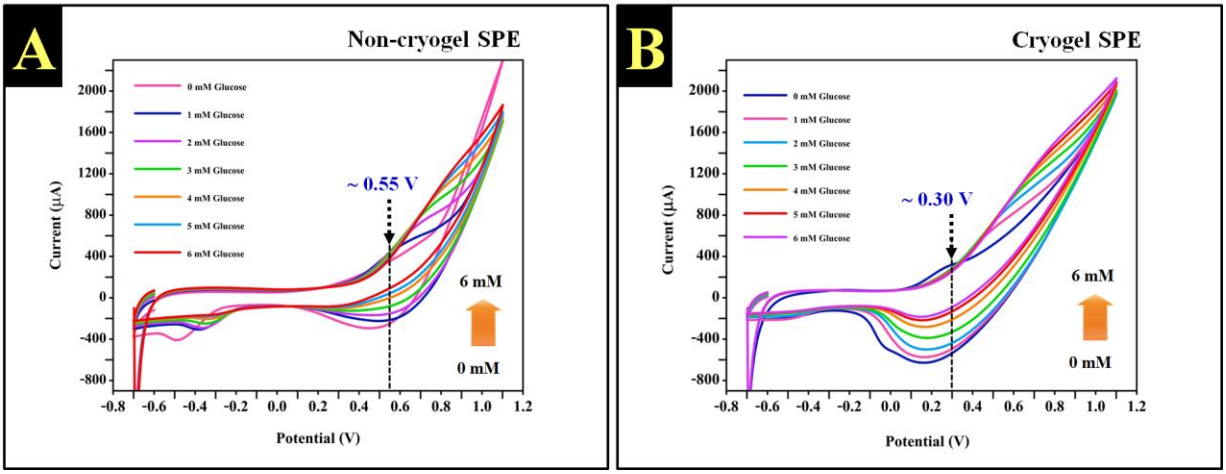

Fig. S4 Relationship between the anodic peak current and the square root of the scan rate ($v^{1/2}$) for glucose oxidation at the CuO@f-MWCNTs–RB cryogel/SPE.

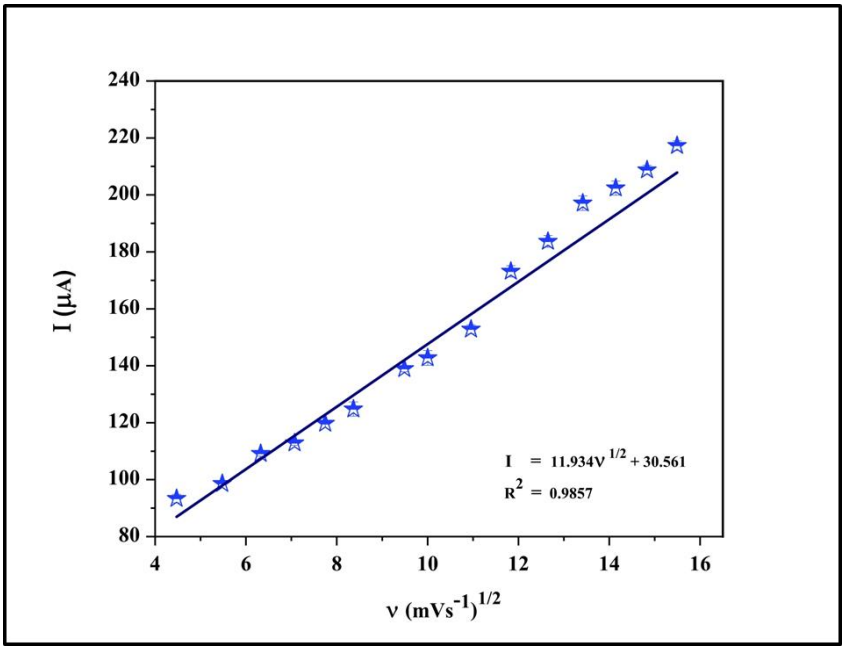

Fig. S5 (A) Sensitivity plots for glucose detection in the concentration range of 0.0 - 6.0 mM obtained using the developed CuO@f-MWCNTs-RB cryogel/SPE by cyclic voltammetry (CV) in NaOH electrolytes with different concentrations (0.01, 0.05, 0.10, 0.15, 0.20, 0.25, and 0.30 M). (B) Sensitivity plots for chronoamperometric glucose detection in the concentration range of 0.0–1.0 mM recorded at different applied potentials (0.10 - 0.70 V) using the CuO@f-MWCNTs-RB cryogel/SPE in 0.20 M NaOH.

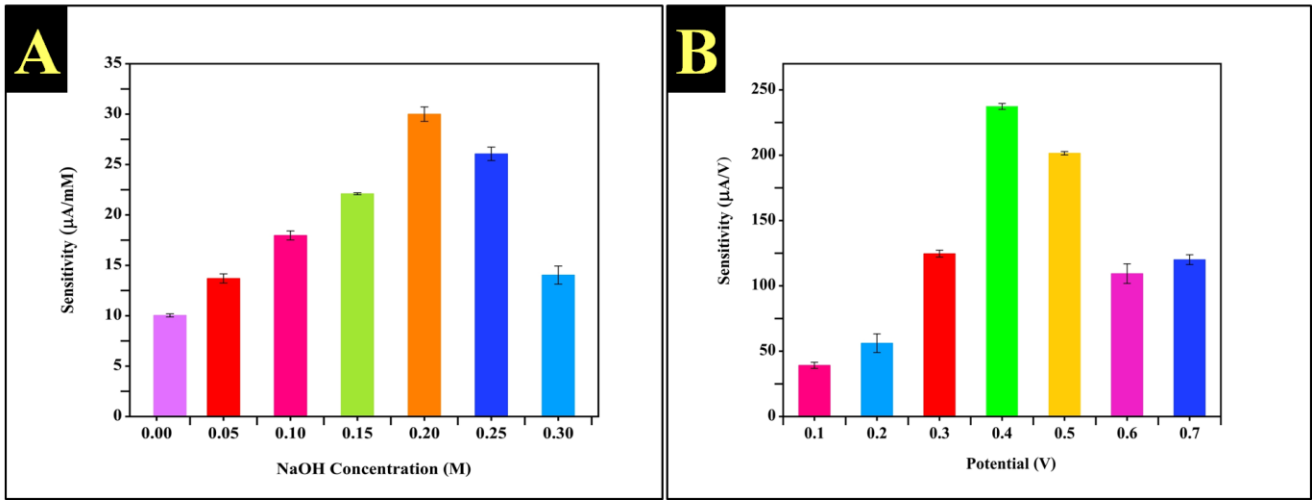

Fig. S6 (A) Repeatability of the CuO@f-MWCNTs–RB cryogel/SPE evaluated by six consecutive chronoamperometric measurements at glucose concentrations of 0.010, 0.50, and 1.0 mM in 0.20 M NaOH at an applied potential of +0.40 V. (B) Reproducibility of the CuO@f-MWCNTs–RB cryogel/SPE assessed using six independently fabricated electrodes for chronoamperometric glucose detection at glucose concentrations ranging from 0.050 to 0.50 mM under identical experimental conditions.

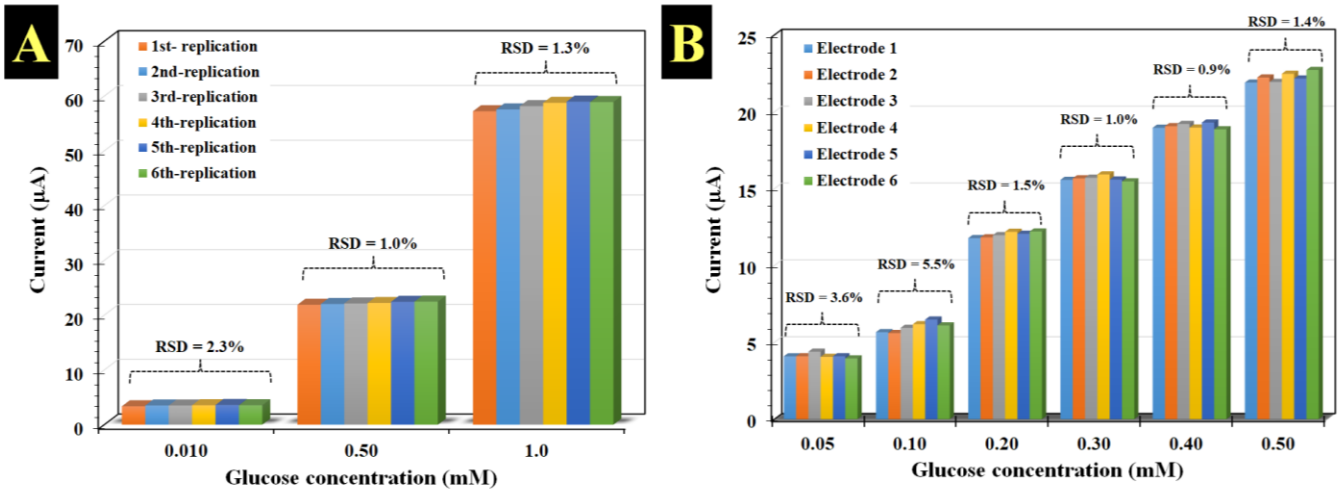

Fig. S7 Cyclic voltammogram obtained from the developed electrode before and after storing under high-humidity conditions for 25 days, recorded in 0.20 M NaOH.

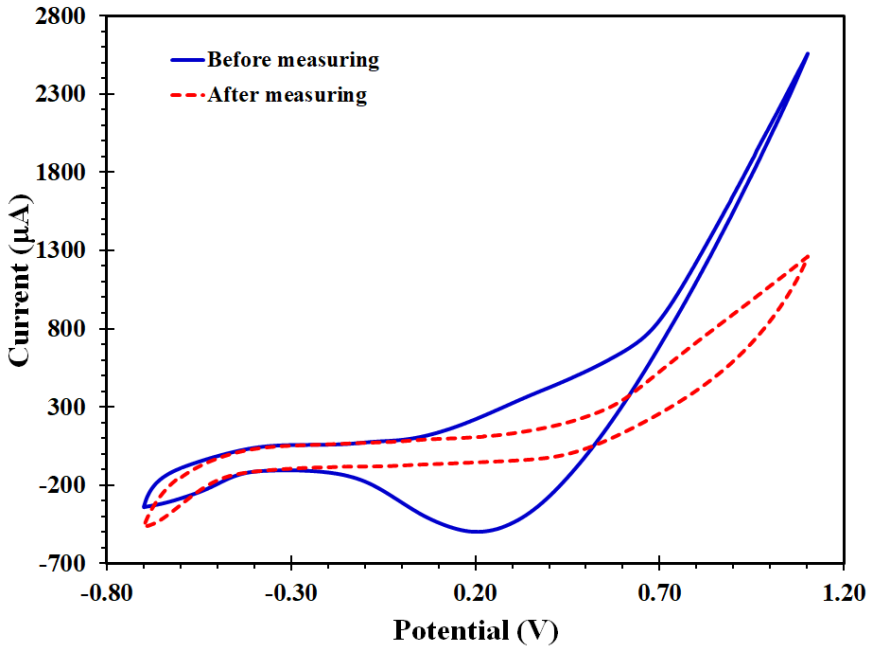

Fig. S8 (A) Amperometric current responses obtained from (a) standard glucose solutions and (b) glucose-spiked plasma samples in the concentration range of 0.05–0.50 mM. (B) Comparison of the corresponding calibration curves derived from standard glucose solutions and glucose-spiked plasma samples measured under identical experimental conditions.

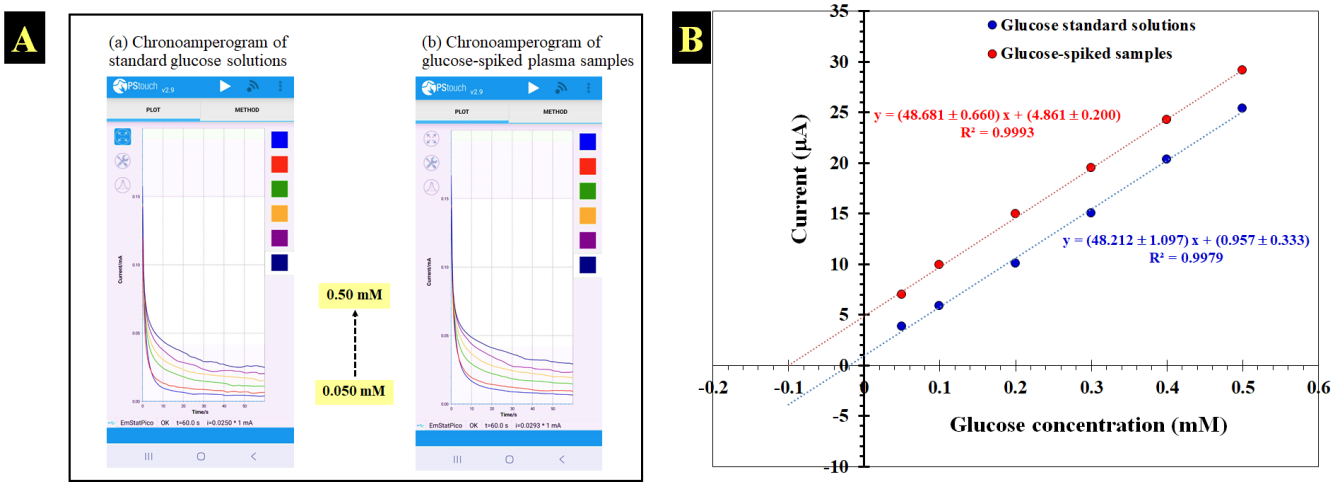

Fig. S9 Bland–Altman plot comparing plasma glucose concentrations determined by the developed CuO@f-MWCNTs–RB cryogel sensor and the reference method. The solid line represents the mean difference (bias), while the dashed lines indicate the limits of agreement (LoA, mean ± 1.96 SD). The calculated LoA ranged from −0.13 mM to +0.08 mM, demonstrating minimal systematic deviation and good agreement between the two methods across the tested concentration range.

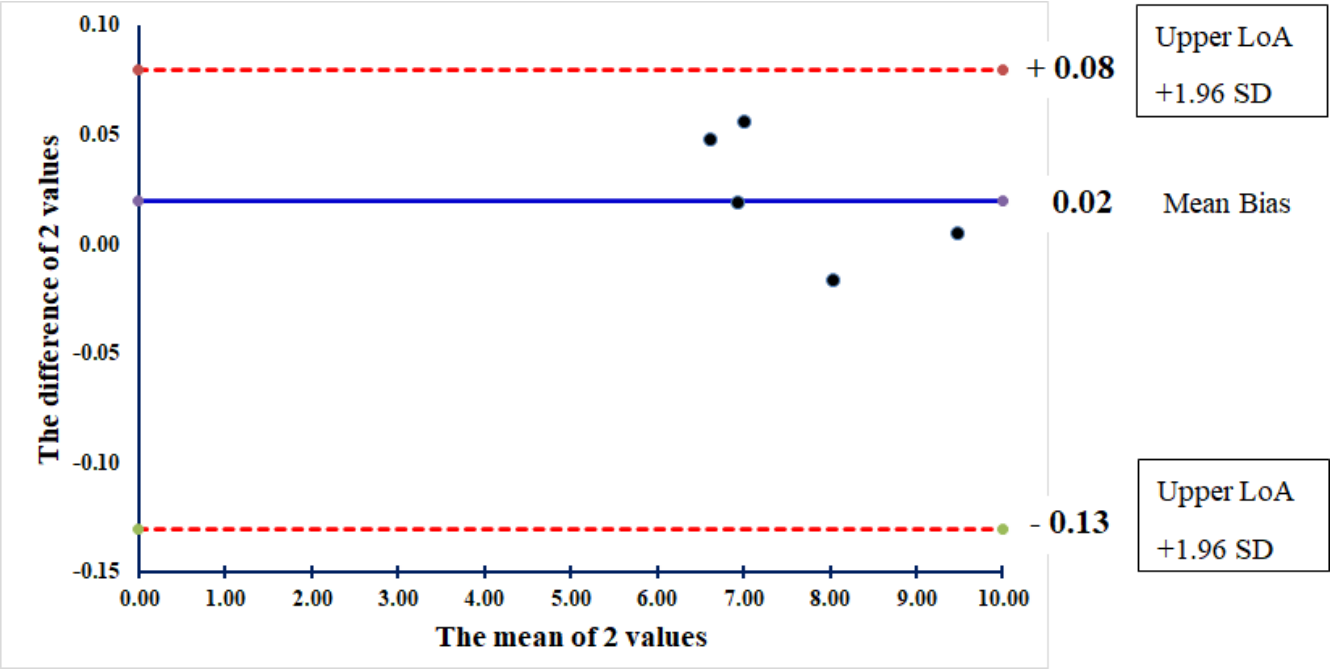

Table. S1 Determination of glucose concentration in real samples

Samples	Glucose concentration (mM)		%Error	%Recovery
	Fabricated sensor	Hospital method		
Plasma 1	7.056	7.00	0.79	100.8
Plasma 2	9.505	9.50	0.05	100.0
Plasma 3	8.043	8.06	0.21	99.8
Plasma 4	6.657	6.61	0.72	100.7
Plasma 5	6.959	6.94	0.27	100.3